Effect of Thermal Bump in Supersonic Flow Control

Hong Yan[1] and Datta Gaitonde[2]
[1]Department of Mechanical and Materials Engineering,
Wright State University, 3640 Colonel Glenn Hwy, Dayton, OH 45435
hong.yan@wright.edu
[2]Air Vehicles Directorate, Air Force Research Laboratory, Wright–Patterson AFB, OH 45433
Datta.Gaitonde@wpafb.af.mil

Abstract

A three-dimensional numerical study is performed to explore the effect of a pulsed rectangular heating element (also denoted as thermal bump) in a Mach 1.5 laminar flat plate boundary layer. The thermal bump is modeled as a time-dependent step surface temperature rise. The thermal bump generates a series of counter-rotating streamwise vortices formed at the four edges of the element. When the bump is pulsed, vortex shedding is observed. These vortices interact with each other, generating a complicated vortical field, and grow in the spanwise direction with the downstream distance. Results show that the vertical perturbation velocity plays a key role in generating a lifting effect to sustain the horizontal disturbances. The streamwise velocity perturbation produces a low-speed region downstream of the centerline and a high-speed region on each side of the bump. The disturbance energy shows that the streamwise kinetic disturbance energy dominates over other components.

1 INTRODUCTION

In recent years, there has been considerable interest in the study of methods to modulate the stability of boundary layers [1, 2, 3, 4, 5, 6, 7, 8, 9]. These studies, overwhelmingly focused on the incompressible regime, have revealed several interesting aspects of bump modulated flows. For example, surface roughness can influence the location of laminar-turbulent transition by two dominating mechanisms. First, they can convert external large-scale disturbances into small-scale boundary layer disturbances, and become possible sources of receptivity. Second, they may generate new disturbances to stabilize or destabilize the boundary layer. Breuer and Haritonidis [1] and Breuer and Landahl [2] performed numerical and experimental simulations to study the transient growth of localized weak and strong disturbances in a laminar boundary layer. They demonstrated that the three-dimensionality in the evolution of localized disturbances may be seen at any stage of the transition process, not confined to the nonlinear development of the flow. For weak disturbances, the initial evolution of the disturbances resulted in the rapid formation of an inclined shear layer, which was in good agreement with inviscid calculation. For strong disturbances, transient growth gives rise to distinct nonlinear effects, and it was found that resulting perturbation depends primarily on the initial distribution of vertical velocity. Gaster et al.[3] reported measurements on the velocity field created by a shallow oscillating bump in a boundary layer. They found that the disturbance was entirely confined to the boundary layer, and the spanwise profile of the disturbance field in the near-field region of the bump differed dramatically from that far downstream. Joslin and Grosch [4] performed a Direct Numerical Simulation (DNS) to duplicate the experimental results by Gaster et al. [3]. In the far field, the bump generated a pair of counter-rotating streamwise vortices just above the wall and on either side of the bump location, which significantly effected the near-wall flow structures. Worner et al. [5] numerically studied the effect of localized hump on the Tollmien-Schlichting waves traveling cross it in a two-dimensional laminar boundary layer. They pointed out that the destabilization by a localized hump was much stronger when its height was increased as opposed to its width. Further, a rounded shape was less destabilizing than a rectangular shape. Researchers have also studied the effect of surface roughness on transient growth. White and Ergin [6] described experiments to explore the receptivity of transient disturbances to surface roughness. The initial disturbances were generated by a spanwise-periodic array of roughness elements. The results indicated that the streamwise flow was

decelerated near the protuberances, but that farther downstream the streamwise flow included both accelerated and decelerated regions. Some of the disturbances produced by the spanwise roughness array underwent a period of transient growth. Fischer and Choudhari [7] presented a numerical study to examine the roughness-induced transient growth in a laminar boundary layer. The results showed that the ratio of roughness size relative to array spacing was a primary control variable in roughness-induced transient growth. Tumin and Reshotko [8] solved the receptivity of boundary layer flow to a three dimensional hump with the help of an expansion of the linearized solution of Navier-Stokes equations into the biorthogonal eigenfunction system. They observed that two counter-rotating streamwise vortices behind the hump entrained the high-speed fluid towards the surface boundary layer. Rizzetta and Visbal [9] used DNS to study the effect of an array of distributed cylindrical roughness elements on flow instability. A pair of co-rotating horseshoe vortices was observed, which did not influence the transition process, while the breakdown of an unstable shear layer formed above the element surface played a strong role in the initiation of transition.

Although the effect of physical bumps on flow instabilities has been studied extensively, far fewer studies have explored the impact of thermal perturbations (thermal bumps). A thermal bump is particularly effective at supersonic and hypersonic speeds. One approach to introduce the bump is through an electromagnetic discharge in which motion is induced by collisional momentum transfer from charged to neutral particles through the action of a Lorentz force [10, 11, 12, 13, 14, 15]. Joule heating is a natural outcome of such interactions, and is the primary agent generated by an electric discharge plasma employed here to influence flow stability.

For supersonic and hypersonic flows, heat injection for control have considered numerous mechanisms, including DC discharges [15], microwave discharges [11] and lasers [14]. Recently however, Samimy et al. [16] have employed Localized Arc Filament Plasma Actuators (LAFPA) in a fundamentally unsteady manner to influence flow stability. The mechanism is to utilize an arc filament initiated between electrodes embedded on the surface to generate rapid (on the time scale of a few microseconds) local heating. The heating causes a local pressure rise, generating streamwise vortices. Samimy et al. [16] employed this method in the control of high speed and high Reynolds number jets. The results showed that forcing the jet with m = 1 mode at the preferred mode frequency provided the maximum mixing enhancement, while significantly reducing the jet potential core length and increasing the jet centerline velocity decay rate beyond the end of potential core.

An alternative approach was described by Visbal et al. [17] who numerically investigated unsteady actuation to trip transitional boundary layers with asymmetric dielectric-barrier-discharge (DBD) actuators. Counter-flow pulsed actuators with intermediate pulsing frequencies were found to be more effective than steady ones to provide an on-demand tripping device for a laminar boundary layer on a flat plate. Yan et al. [18, 19] studied the steady heating effect on a Mach 1.5 laminar boundary layer. Far downstream of the heating, a series of counter-rotating streamwise vortices were observed above the wall and on the each side of the heating element in the spanwise direction. These recent studies present a new concept of thermal bump, which can be generated by localized arc discharge or DBD actuators. Advantages of thermal bumps over physical ones include the ability to switch on and off on-demand, but also the ability, in principle, to pulse at any desired frequency combination.

This paper explores thermal perturbation as a flow control concept in a supersonic boundary layer. First, a no-heating basic state is simulated to ensure an accurate unperturbed basic state. Then, detailed analyses are presented for a pulsed thermal bump with focus on the instantaneous flow structures in the early stage of disturbance propagation.

2. FLOW CONFIGURATION

A Mach 1.5 flat plate flow is considered with the total temperature and pressure of 325 K and 3.7×10^5 Pa, respectively. The rectangular thermal bump is centered in the spanwise direction as shown schematically in Figure 1. The bump width and length are set to be w =1 mm and 0.2 mm in the spanwise and streamwise direction, respectively. The heating effect is modeled as a time-dependent step surface temperature rise ΔT_w with a monochromatic pulsing frequency (f) and duty cycle as shown in Figure 2, where the pulsing time period $t_T = 1/f$. The subscript w denotes the value at the wall. For simplicity, it is assumed that $\Delta T_w = T_w - T_{w0}$, where T_w and T_{w0} are wall temperature inside and outside of the heating region, respectively, and T_{w0} is fixed at the adiabatic temperature (T_{ad}) as shown in Figure 1. The bump pulses at f = 100 kHz with duty cycle of 0.5 and $T_w = 1.4\,T_{ad}$.

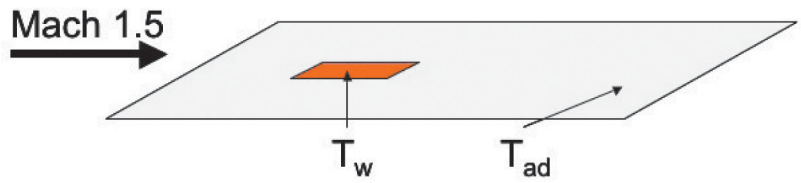

Figure 1. Flat plate with thermal bump

In all the perturbed simulations, the thermal bump is placed immediately upstream of the first neutral point in the stability neutral curve for an adiabatic flat plate boundary layer with the freestream Mach number (M_∞) of 1.5. The stability diagram, shown in Figure 3, is obtained from the Langley Stability and Transition Analysis Codes (LASTRAC) [20]. LASTRAC performs linear calculations and transition correlation by using the N-factor method based on linear stability theory. The N factor is defined by $N = \int_{s_0}^{s_1} \gamma ds$, where s_0 is the point at which the disturbance first begins to grow, s_1 is the point at which transition is correlated, and γ is the characteristic growth rate of the disturbance. For disturbances at f = 100 kHz, the first neutral point is located at Re = 610 based on the similarity boundary-layer length scale defined as $\sqrt{\nu_\infty x/u_\infty}$, where ν_∞ and u_∞ are the dynamic viscosity and streamwise velocity at freestream, respectively and is shown as the solid rectangle in Figure 3. The local Reynolds number based on the running distance from the leading edge of the plate is defined by $Re_x = Re^2$. Thus, the distance from the leading edge of the plate to the leading edge of the heating element is 7.65 mm (i.e. corresponding to Re = 610).

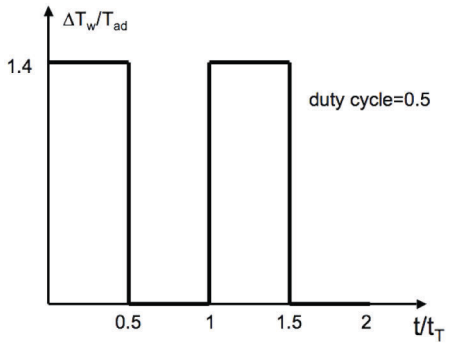

Figure 2. Two time periods of surface temperature rise

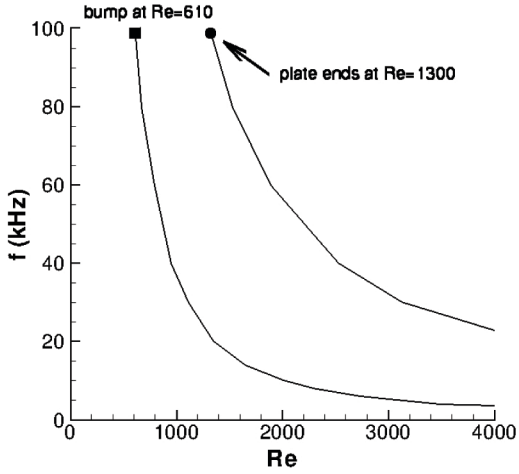

Figure 3: Neutral curve for Mach 1.5 adiabatic flat plate boundary layer

3. NUMERICAL MODEL

The Cartesian coordinate system is adopted with $x,\ y$ and z in the streamwise, wall-normal and spanwise direction, respectively. The x axis is placed through the center of the plate with the origin at the leading edge of the plate. The computational domain is L_x =38 mm long, L_y =20 mm high and L_z =3 mm wide. This is determined by taking two factors into consideration. In the streamwise direction, the domain is long enough to capture 3D effects induced by heating and to eliminate the non-physical effects at the outflow boundary. Based on this constraint, the Reynolds number at the trailing edge of the plate is $Re_L = 1.8 \times 10^6$ (i.e. $Re = 1300$), which is immediately downstream of the second neutral point and is marked as the solid circle in Figure 3. In the vertical direction, the domain is high enough to avoid the effect of the reflection of the leading edge shock onto the surface. The upper boundary is positioned at $86\delta_L$ above the wall, where δ_L is the boundary layer thickness at the trailing edge of the plate.

The grid, comprised of $265 \times 277 \times 57$ points in the $x,\ y$ and z direction, respectively, is refined near the leading edge of the flat plate and in the vicinity of the thermal bump. Approximately 150 grid points are employed inside the boundary layer at the leading edge of the heating element to resolve the viscous layer and capture the heat release process.

The third-order accurate Roe scheme is used with the Min-Mod limiter in each direction, and the fourth-order accurate Runge-Kutta scheme is applied for time integration. The sudden temperature rise in the heating area reduces the allowable time step by increasing the speed of sound based on Courant-Friedrichs-Lewy (CFL) criterion which restricts the stable time step in explicit formulations [21]. The time step is fixed at 5×10^{-10}s. For reference, one characteristic time for the flow to transverse the whole plate at the freestream velocity is 8×10^{-6} s.

For boundary conditions, the stagnation temperature and pressure and Mach number are fixed at the inflow. The non-slip condition with a fixed wall temperature is used on the wall. The symmetry condition is enforced at the spanwise boundary to simulate spanwise periodic series of heating element spaced L_z apart. First-order extrapolation is applied at the outflow and upper boundaries.

4. NUMERICAL RESULTS

The discussion is organized as follows: First, the accuracy of the no-heating basic state is established by comparing with theoretical compressible results. Then, the heating case is discussed in terms of the flow structures observed as well as disturbance quantities obtained.

4.1 Unperturbed Flow (Basic State)

The basic state is a Mach 1.5 adiabatic flat plate boundary layer with Reynolds number at the trailing edge of the plate of $Re_L = 1.80 \times 10^6$. Figure 4 shows the surface density and pressure distribution along the x direction, where the subscript ∞ denotes the freestream condition. An initial pressure rise is caused by a leading edge shock formed due to boundary layer displacement at the leading edge. This feature becomes weaker till the shock evolves into Mach wave with the angle of 41.8˚ based on M_∞ as it extends away from the plate as seen in Figure 5. According to classic hypersonic flow theory by

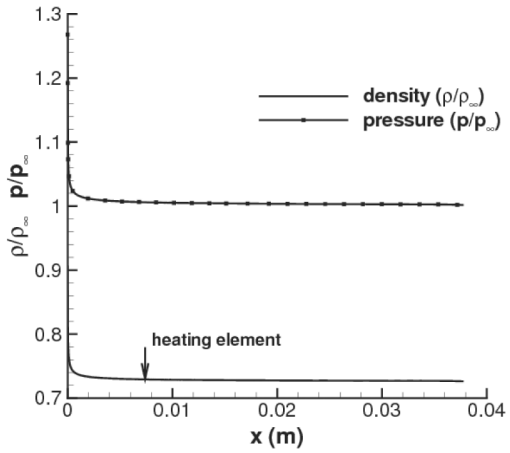

Figure 4. Surface density (ρ) and pressure (p) along the centerline (basic state)

Hayes and Probstein [22], the pressure distribution near the leading edge of a solid surface can be significantly altered by the growth rate of the displacement thickness of a boundary layer. The pressure interaction parameter is defined by $\bar{\chi} = M_\infty^3 \ (C/Re_x)^{1/2}$, where $C = (\mu_w \rho_w)/(\mu_\infty \rho_\infty)$. The flow undergoes viscous interaction at the leading edge of the plate, resulting in the flow compression. Finally, the surface pressure levels off slightly above the freestream value due to the effect of the leading edge shock. The heating element is placed away from the interaction region as shown in Figure 4, which also indicates that the surface density is below the freestream value because the wall is hotter than the freestream under adiabatic conditions and pressure varies only modestly cross the boundary layer.

Figure 5 also shows that the Mach wave ripples in the region far away from the wall due to large grid stretching in the y direction, which is used to extend the upper boundary at reasonable computational cost. To demonstrate that the reflection of this feature from the upper boundary is inconsequential to the current results, Figure 6 shows the pressure profiles along the x direction at three y locations, where 0 is the boundary layer thickness at the leading edge of the heating element. At each y location, the pressure exhibits two peaks. The initial peak is caused by the leading edge shock, while the second one is caused by the reflection of the Mach wave from the upper boundary. The second peak is much weaker than the first one, explaining its absence in the contour plot. The effect of the reflection becomes weaker as y decreases (i.e. moves away from the upper boundary). As discussed later, the complex vortex interaction occurs within $y = 20\delta_0$ where the effect of the reflection is negligible as shown in Figure 6.

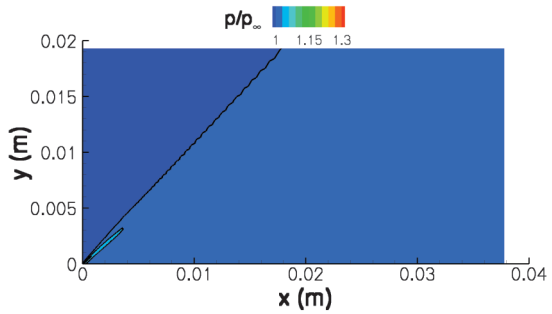

Figure 5. p contours on the center plane (basic state)

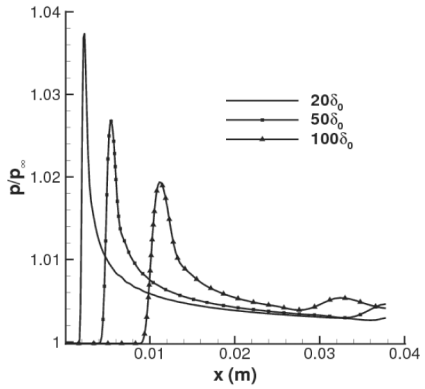

Figure 6. p along the x direction at different y locations (basic state)

Figures 7 and 8 show the streamwise velocity and temperature profiles along the y direction at the leading edge of the location where the heating element will be placed. The comparisons with the compressible theoretical profiles are good in terms of the profile shape and boundary layer thickness.

Figure 9 shows the predicted friction coecient along the x direction, and the good agreement is made with the theoretical profile, which is obtained from $c_f = \dfrac{0.664\sqrt{C*}}{\mathrm{Re}_x^{1/2}}$. The compressibility effect is

factored in by the Chapman-Rubesin parameter (C^*) [23] computed through the approximated reference temperature ratio proposed by Eckert [24].

The basic state simulation captures the prominent features of the compressible flat plate boundary layer and provides an accurate unperturbed basic state to study the effect of the thermal bump.

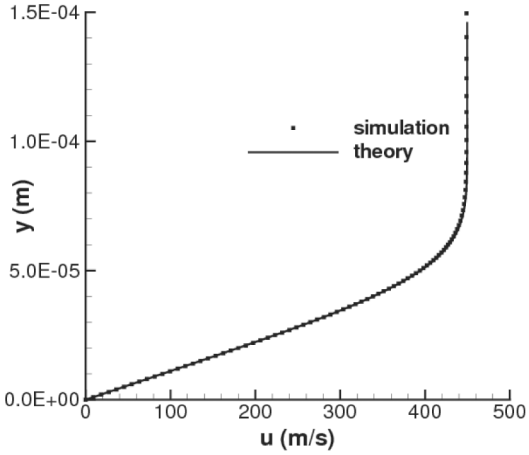

Figure 7. Streamwise velocity (u) in the y direction (basic state)

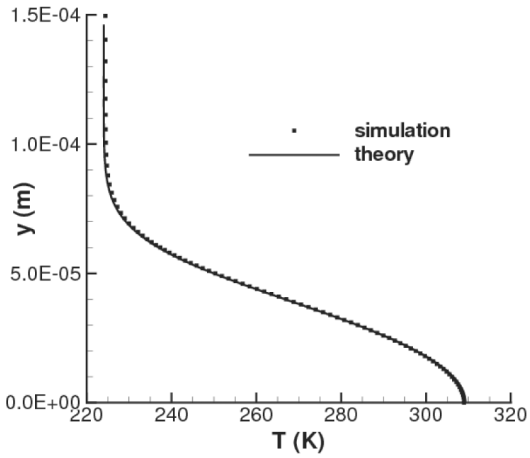

Figure 8. Static temperature (T) in the y direction (basic state)

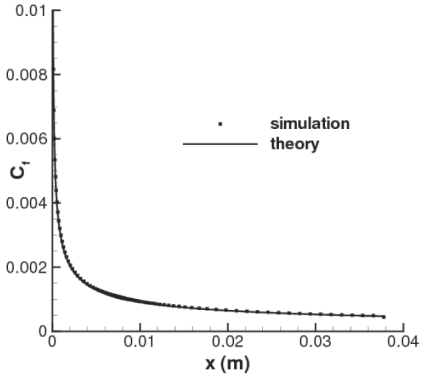

Figure 9. Skin friction coefficient (c_f) in the x direction (basic state)

4.2 Heating Effect

The simulation runs for ten pulsing periods. The signature of the vortex interaction from the previous pulsing periods remains in the downstream locations.

4.2.1 Perturbed Flow Structures

The sudden heat release acts as an isolated thermal bump on the surface, which produces disturbances of three-dimensional nature. The surface pressure along the centerline is shown in Figure 10 for $t = 0.1t_T$. The initial surface pressure rise is caused by the leading edge shock due to the viscous/inviscid interaction as discussed earlier in Section 4.1. A weak shock is formed at the leading edge of the thermal bump and is followed by the expansion waves at the trailing edge. The pressure variation remains of the same intensity between the surface and $y = \delta_0$ with a small phase change as indicated in Figure 10.

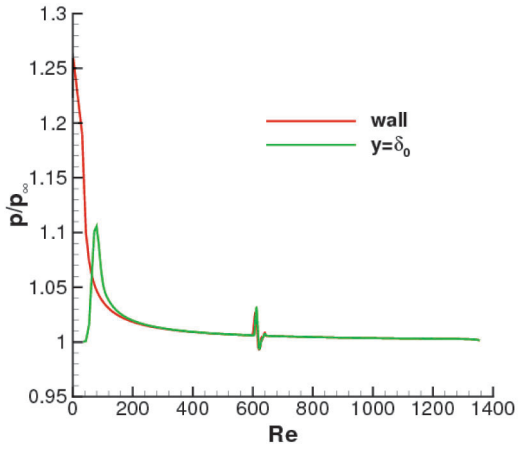

Figure 10. Instantaneous p in the x direction at $t = 0.1t_T$

The perturbed pressure field generates complex vortical structures downstream of the thermal bump. Figure 11 shows the instantaneous streamwise vorticity contours on the wall. When the bump is just turned on (i.e. $t = 0.1t_T$), two pairs of strong counter-rotating streamwise vortices are formed at the edges of the heating element as shown in Figure 11(a). Close examination of each vorticity term reveals that the variation of the spanwise velocity in the y direction is a main contributor. The vortices are observed shedding simultaneously as the thermal bump pulses and its induced disturbances propagate downstream, which is shown in Figure 11(b) at $t = 9.1t_T$. The vortical structures with the alternating signs are clearly seen. The vorticity intensity decays significantly after Re = 900 as a result of spanwise velocity decay.

The disturbances penetrate into the boundary layer. Figure 12 shows the instantaneous streamwise vorticity contours on the $z = -0.5w$ plane, where δ_0^* is the displacement thickness at the leading edge of the thermal bump. The alternating vortical structures are confined to the boundary layer and are steeper at the leading edge of the thermal bump due to the effect of the heating induced shock. As they move downstream, the upper portion of the structures tilt in parallel with an angle of about 2° to the x direction and the ω_x intensity decreases in the y direction. The y axis is artificially stretched to highlight the feature. Meanwhile the vortices grow in the z direction and disperse laterally as shown in Figure 13 at $y = \delta_0^*$ away from the wall, forming a swept-front resembling waves from a point source. The vortex splitting is observed at Re = 700 where two consecutive positive and negative rotating vortices appear around $z = 0.5w$ and $z = -0.5w$, respectively. This is caused by the complex vortex/boundary layer interaction above the wall.

The vortical structures distort the mean flow, producing a low-speed region downstream of the centerline and high-speed regions on either side of the bump as seen in Figure 14, where the time-mean streamwise velocity $(\bar{u})$ contours are shown in two downstream locations. The y axis, η, is the dimensionless similarity variable defined as $\eta = y\sqrt{u_\infty / 2\nu_\infty x}$. This effect was experimentally observed in the study of the transient growth due to three-dimensional disturbances produced by the stationary roughness [25]. It is seen that the velocity deficit and excess regions grow in size in the x direction, which is discussed in detail in Figure 15.

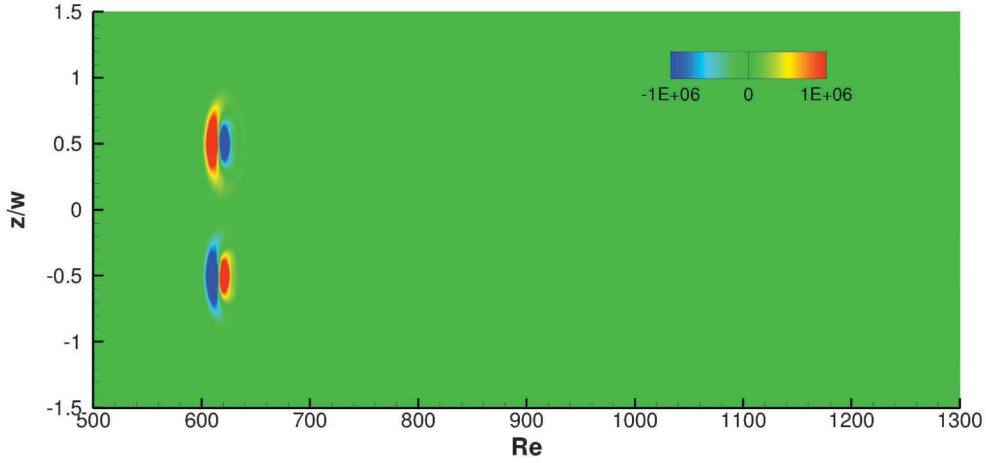

(a) $t = 0.1t_T$

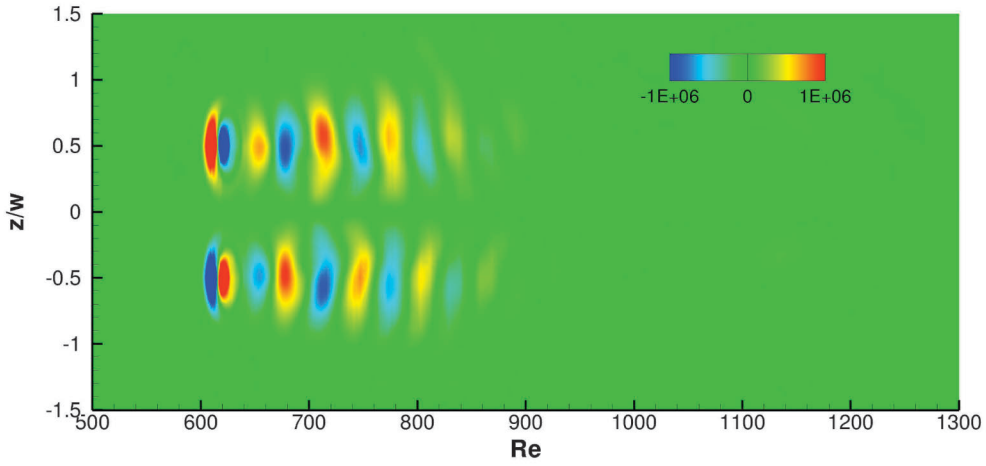

(b) $t = 9.1t_T$

Figure 11. Instantaneous streamwise vorticity (w_x) contours on the wall

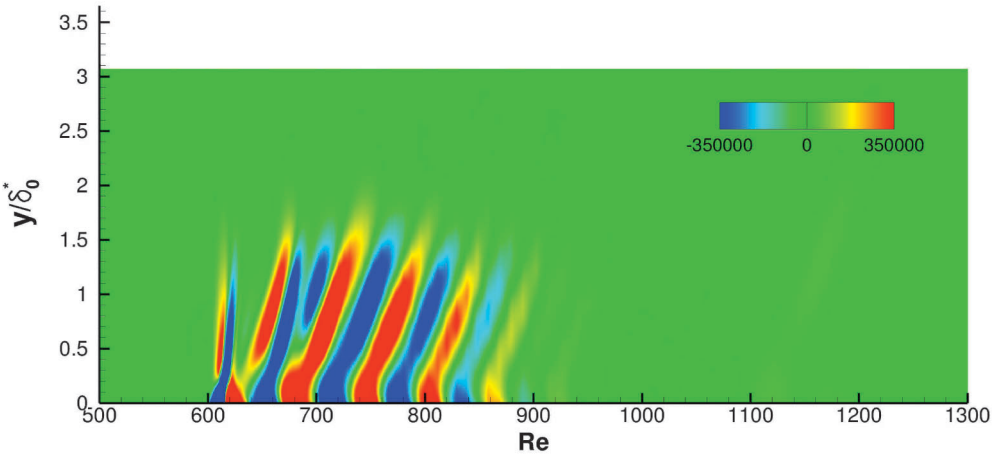

Figure 12. ω_x contours on $z = -0.5w$ at $t = 9.1t_T$

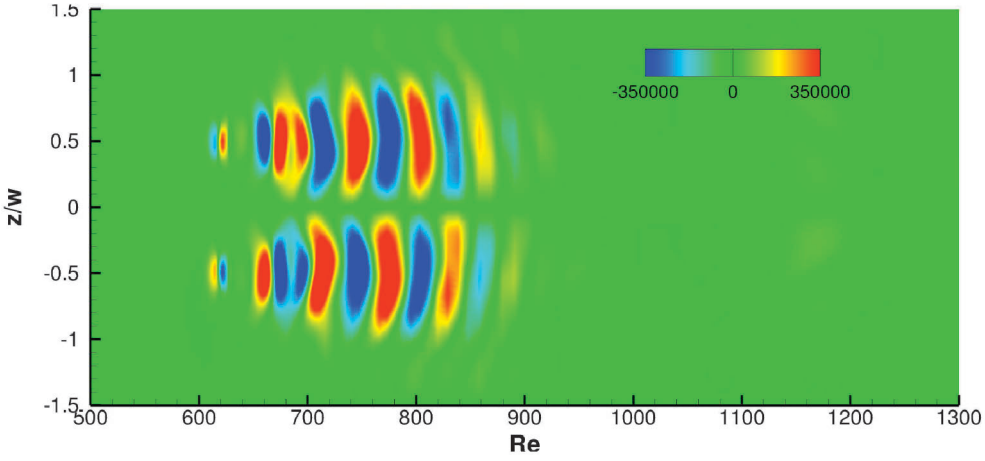

Figure 13. ω_x contours on $y = \delta_0^*$ at $t = 9.1t_T$

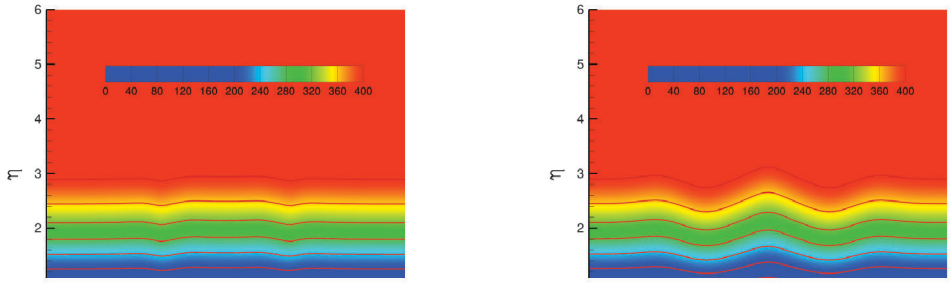

(a) Re = 695 (b) Re = 1054

Figure 14. Time-mean streamwise velocity ($\bar{u}$) contours

The variation of the intensity of the low-speed and high-speed regions with the downstream distance is shown in Figure 15 on $y = \delta_0^*$. The non-dimensional $\bar{u}$ perturbation is defined as $u'_m = (\bar{u} - u_b)/u_\infty$, where the subscript b denotes the basic state case. In the near-wake of the thermal bump at Re = 619 and 695, u'_m does not level off to zero at the spanwise boundaries, indicating a strong and laterally spreading perturbation. At Re = 695, a low-speed region and two high-speed regions start to form. The intensity of the velocity deficit and excess increases from Re = 695 to Re = 915. However a different behavior is observed in the far downstream locations where the intensity decreases from Re = 915 to Re = 1184, and the perturbation levels off to zero at the spanwise boundaries. The phenomenon of the intensity decay in the far-wake region is consistent with the studies by Joslin and Grosch [4].

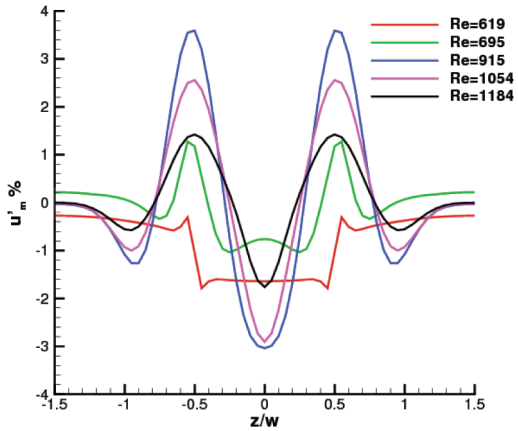

Figure 15. Time-mean streamwise velocity perturbation (u'_m) in the z direction

As shown above, the initial disturbance is of three-dimensional nature. Landahl [26] showed that for three-dimensional initial disturbances, the integrated effect of the vertical perturbation velocity (v') termed as "liftup" in the presence of the mean shear created a horizontal disturbance velocity which did not vanish for long times. Figure 16 shows the three components of the perturbation velocity ($\vec{u}_0 = \vec{u} - \vec{u}_b$) contours on $y = 0$ at $t = 9.1t_T$. The "liftup" term produces the horizontal disturbance velocities (u' and w'). It is evident that v' decays at a faster rate than u' and w'. This finding resembles the results by Breuer and Haritonidis [1] who studied the effect of a three- dimensional disturbance in incompressible laminar boundary layer and found that u' and w' still grew as v' decayed, and confirms the importance of the initial vertical velocity perturbation in the growth of the disturbance energy

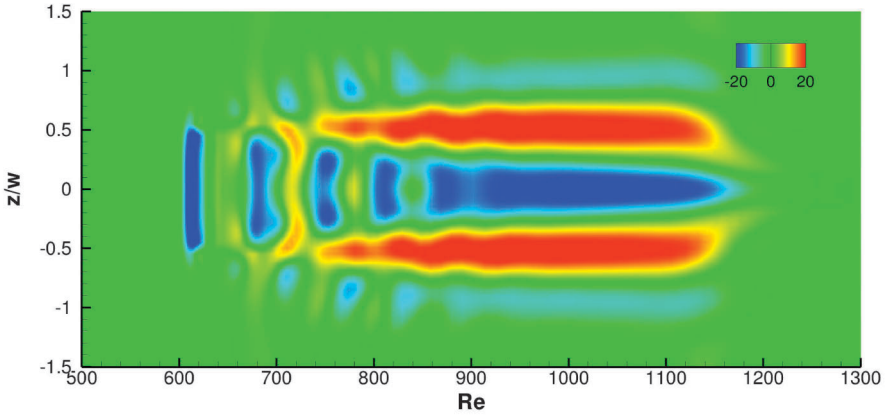

(a) streamwise velocity perturbation (u')

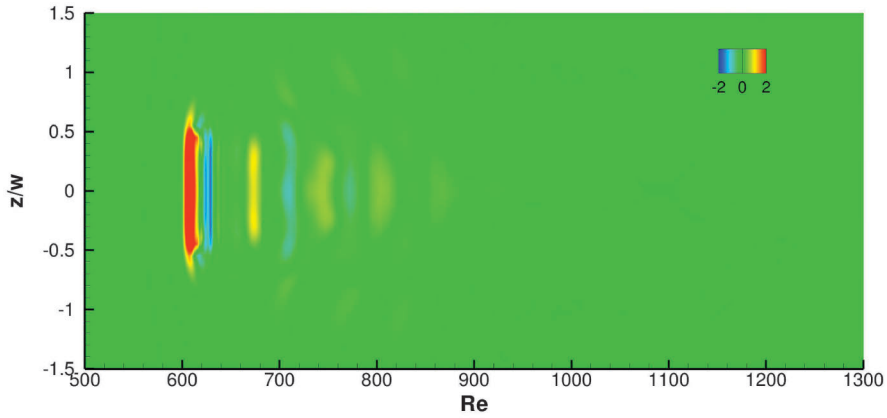

(b) wall-normall velocity perturbation (v')

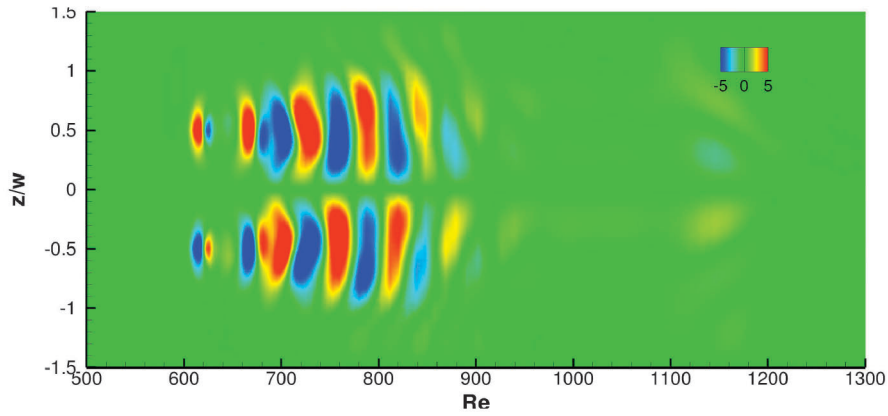

(c) spanwise velocity perturbation (w')

Figure 16. Instantaneous contours on y = 0 at $t = 9.1t_T$

shown by Landahl [27]. The similar pattern of w' to ω_x confirms that the spanwise velocity variation is a main contributor to ω_x.

Figure 17 shows the u' and v' contours on the center plane. The most noticeable difference is that u' is confined to the near-wall region, while v' is spread vertically through the whole domain. This observation was analyzed by Breuer and Haritonidis [1] using the linear theory. The liftup term generated u' and was only non-zero where there was a mean shear, so u' was expected not to extend beyond the region of mean shear. An alternating high-speed and low-speed region is seen for both components. In u', the low-speed region grows in size in the downstream. It is also noted that the u' is stretched and tilted over. Breuer and Haritonidis [1] explained it as the characteristics of the transient part of the disturbance. Because the transient part travels at the local mean velocity, the upper portion advects faster than the portion closer to the wall, resulting in the tilting of u'.

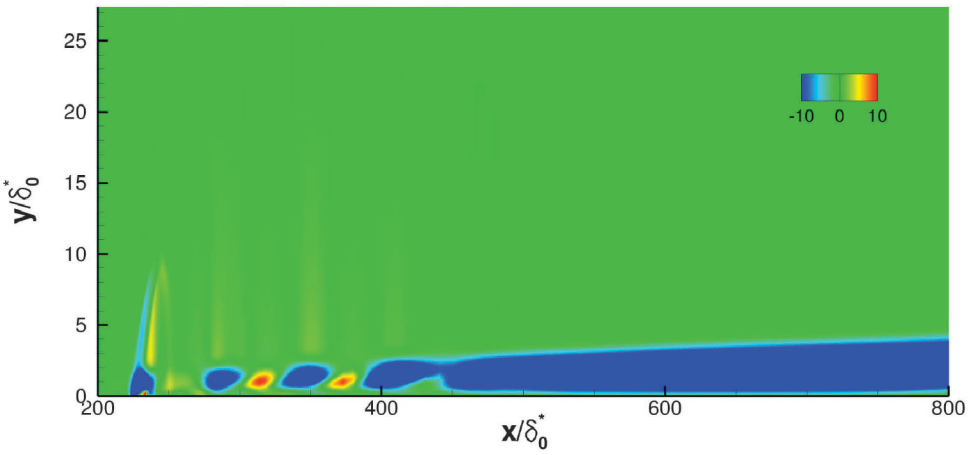

(a) u'

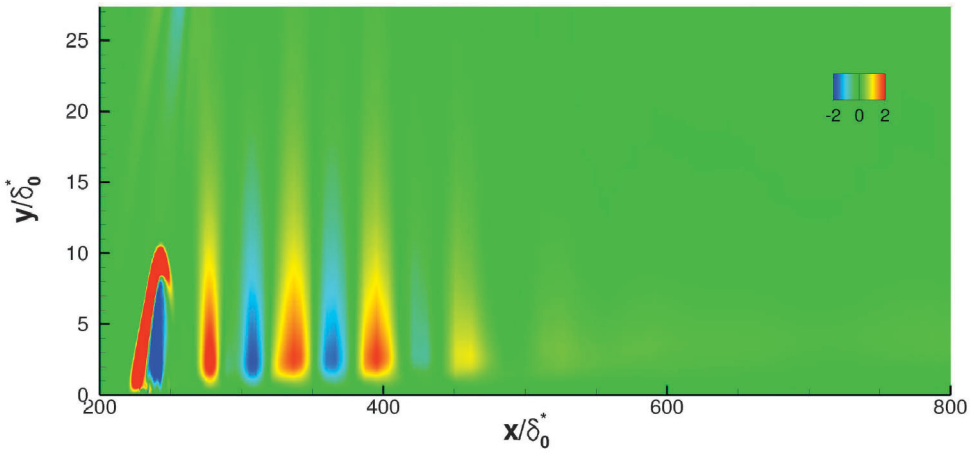

(b) v'

Figure 17. Instantaneous contours on z = 0 at $t = 9.1t_T$

The strength of disturbance energy growth can be measured by the energy norm proposed by Tumin and Reshotko [28] as

$$E = \int_0^\infty \vec{q}^T A \vec{q} dy \tag{1}$$

where $\vec{q}$ and A are the perturbation amplitude vector and diagonal matrix, respectively, and are expressed as

$$\vec{q} = (u', v', w', \rho', T')^T \tag{2}$$

$$A = diag[\rho, \rho, \rho, T/(\gamma \rho M_\infty^2), \rho/(\gamma(\gamma-1)TM_\infty^2)] \tag{3}$$

where the superscript $'$ represents the deviation of the instantaneous perturbed flow from the basic state. The first three terms represent the components of the kinetic perturbation energy denoted as E_u, E_v and E_w, respectively and the last two represent the thermodynamic perturbation energy components as E_ρ and E_T. Figure 18 shows the three components of the kinetic energy along the x direction. Because the flow is symmetric about $z = 0$, E_w is plotted at $z = -0.5w$ and other energy variables are at $z = 0$. Local peak value occurs in the vicinity of the heating as expected. As the thermal bump pulses, the disturbance propagates downstream and oscillates as seen in the ripples downstream. After Re=900, both E_v and E_w decay significantly, while E_u undergoes a significant increase. The peak E_u is one order of magnitude higher than the other two components and increases as it moves downstream with the pulsing as shown in Figure 19. This indicates that pulsing acts as an energy supplier to the disturbances. The thermodynamic energy (E_ρ and E_T) is observed to increase sharply in the vicinity of the heating region and dissipates faster downstream as shown in Figure 20. Their peak values are two orders of magnitude lower than E_w. The total disturbance energy (E) behaves similarly to E_w since E_w dominates over other components.

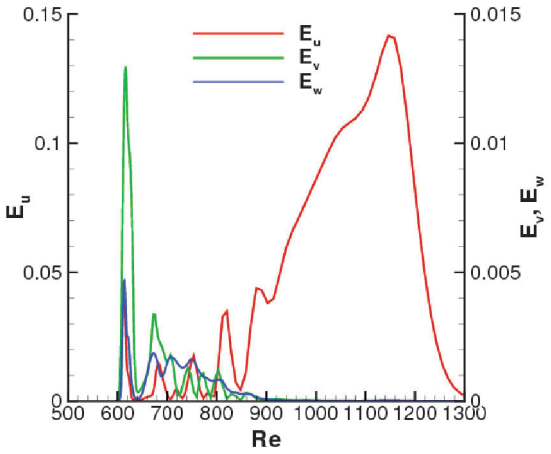

Figure 18. E_u, E_v and E_w at $t = 9.1t_T$

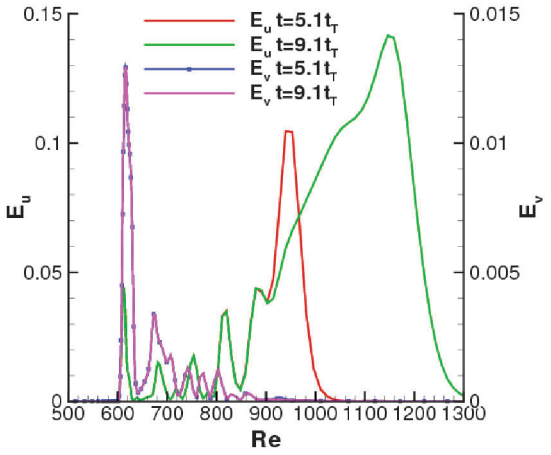

Figure 19. E_u and E_v at $t = 5.1t_T$ and $t = 9.1t_T$

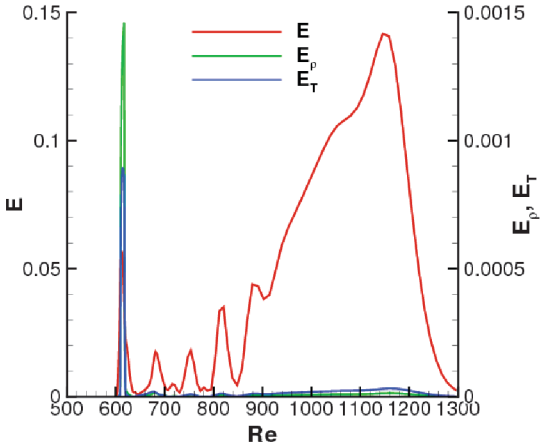

Figure 20. E, E_ρ and E_T at $t = 9.1t_T$

5. CONCLUDING REMARKS

The flow structures generated by a pulsed thermal bump were analyzed through a three-dimensional simulation of a Mach 1.5 flat plate boundary layer. The no-heating basic state was accurately predicted by comparing with the theoretical profiles. In heating study, strong vortex shedding was observed in the near field and decayed much faster after about $Re = 900$ as a result of spanwise velocity decay. Nonlinear flow development caused the mean flow distortion, generating velocity excess and deficit regions downstream of the bump. The vertical perturbation velocity generated a lifting effect to energize the horizontal disturbance and pulsing plays an important role in sustaining the disturbance grow.

6. ACKNOWLEDGMENTS

This research was supported by AFOSR under tasks monitored by Dr. John Schmisseur and Dr. Fariba Fahroo. This work was partially supported by the National Center for Supercomputing Applications under grant CTS030001 and utilized the NCSA Xeon Linux Supercluster.

REFERENCES

[1] Breuer, K. S. and Haritonidis, J. H., "The Evolution of a Localized Disturbance in a Laminar Boundary Layer. Part I. Weak Disturbances," *J. Fluid Mech.*, Vol. 220, 1990, pp. 569-594.

[2] Breuer, K. S. and Landahl, M. T., "The Evolution of a Localized Disturbance in a Laminar Boundary Layer. Part I. Strong Disturbances," *J. Fluid Mech.*, Vol. 220, 1990, pp. 595-621.

[3] Gaster, M., Grosch, C. E., and Jackson, T. L., "The Velocity Field Created by a Shallow Bump in a Boundary Layer," Phys. Fluids, Vol. 6, No. 9, 1994, pp. 3079-3085.

[4] Joslin, R. D. and Grosch, C. E., "Growth Characteristics Downstream of a Shallow Bump: Computation and Experiment," *Phys. Fluids*, Vol. 7, No. 12, 1995, pp. 3042-3047.

[5] Worner, A., Rist, U., and Wagner, S., "Humps/Steps Influence on Stability Characteristics of Two-Dimensional Laminar Boundary Layer," *AIAA J.*, Vol. 41, No. 2, 2003, pp. 192-197.

[6] White, E. B. and Ergin, F. G., "Receptivity and Transient Growth of Roughness-Induced Disturbances," AIAA Paper 2003-4243 , 2003.

[7] Fischer, P. and Choudhari, M., "Numerical Simulation of Roughness-Induced Transient Growth in a Laminar Boundary Layer," AIAA Paper 2004-2539 , 2004.

[8] Tumin, A. and Reshotko, E., "Receptivity of a Boundary-Layer Flow to a Three-Dimensional Hump at Finite Reynolds Numbers," *Phys. Fluid*, Vol. 17, No. 9, 2005, pp. 094101.

[9] Rizzetta, D. P. and Visbal, M. R., "Direct Numerical Simulations of Flow Past an Array of Distributed Roughness Elements," AIAA Paper 2006-3527 , 2006.

[10] Roth, J. R., Sherman, D. M., and P, W. S., "Electrohydrodynamic Flow Control with a Glow Discharge Surface Plasma," *AIAA J.*, Vol. 38, No. 7, 2000, pp. 1166-1172.

[11] Leonov, S., Bityurin, V., Savischenko, N., Yuriev, A., and Gromov, V., "Influence of Surface Electrical Discharge on Friction of Plate in Subsonic and Transonic Airfoil," AIAA Paper 2000-0640 , 2001.

[12] Shang, J. S., "Plasma Injection for Hypersonic Blunt Body Drag Reduction," *AIAA J*., Vol. 40, 2002, pp. 1178-1186.

[13] Enloe, C. L., Mclaughlin, T. E., Vandyken, R. D., Kachner, K. D., Jumper, E. J., C, C. T., Post, M., and Haddad, O., "Mechanisms and Responses of a Single Dielectric Barrier Plasma Actuator: Geometric Effects," *AIAA J*., Vol. 42, 2004, pp. 595-604.

[14] Adelgren, R., Yan, H., Elliott, G., Knight, D., Beutner, T., and Zheltovodov, A., "Control of Edney IV Interaction by Pulsed Laser Energy Deposition," *AIAA J*., Vol. 43, No. 2, 2005, pp. 256-269.

[15] Shang, J. S., Surzhikov, S. T., Kimmel, R., Gaitonde, D., Menart, J., and Hayes, J., "Mech-anisms of Plasma Actuators for Hypersonic Flow Control," *Progress in Aerospace Sciences*., Vol. 41, 2005, pp. 642-668.

[16] Samimy, M., Kim, J.-H., I, A., J-H, K., Utkin, Y., and S, K., "Active Control of High Speed and High Reynolds Number Free Jets Using Plasma Actuators," AIAA Paper 2006-0711 , 2006.

[17] Visbal, M. R., Gaitonde, D. V., and Roy, S., "Control of Transitional and Turbulent Flows Using Plasma-Based Actuators," AIAA Paper 2006-3230 , 2006.

[18] Yan, H., Gaitonde, D., and Shang, J., "Investigation of Localized Arc Filament Plasma Actuator in Supersonic Boundary Layer," AIAA Paper 2007-1234 , 2007.

[19] Yan, H., Gaitonde, D., and Shang, J., "Numerical Investigation of Pulsed Thermal Perturbation in Supersonic Boundary Layer," AIAA Paper 2007-3887 , 2007.

[20] Chang, C. L., "Langley Stability and Transition Analysis Code (LASTRAC) Version 1.2 User Manual," NASA/TM-2004-213233, 2004.

[21] Tannehill, J., Anderson, D. A., and Pletcher, R. H., *Computational Fluid Mechanics and Heat Transfer*, second edition, Taylor & Francis, PA, 1997.

[22] Hayes, W. and Probstein, R., Hypersonic Flow Theory, Academic, New York, 1959.

[23] Chapman, D. R. and Rubesin, M. W., "Temperature and Velocity Profiles in the Compressible Laminar Boundary Layer with Arbitrary Distribution of Surface Temperature," *J. Aeronaut. Sci*., Vol. 16, No. 9, 1949, pp. 547-565.

[24] Eckert, E. R. G., "Engineering Relations for Friction and Heat Transfer to Surfaces in High Velocity Flow," *J. Aeronatu. Sci*., Vol. 22, 1955, pp. 585-587.

[25] White, E. B., "Transient Growth of Stationary Disturbances in a Flat Plate Boundary Layer," *Physics of Fluids*, Vol. 14, No. 12, 2002, pp. 4429-4439.

[26] Landahl, M. T., "Wave Breakdown and Turbulence," *SIAM J. Appl. Maths*., Vol. 28, 1975, pp. 735-756.

[27] Landahl, M. T., "A Note on an Algebraic Instability of Inviscid Parallel Shear Flows," *J. Fluid Mech*., Vol. 98, 1980, pp. 243-251.

[28] Tumin, A. and Reshotko, E., "Spatial Theory of Optimal Disturbances in Boundary Layers," *Phys. Fluid*, Vol. 13, No. 7, 2001, pp. 2097-2104.